

# Unveiling the Capacitive Performance of Electrochemically Engineered Anatase-Polypyrrole/ITO Films: Electrochemical, Microscopic, and Spectroscopic Inspections

Fahim Hamidouche<sup>1,2</sup>, Kaouthar Bouguerra<sup>1</sup>, Zohra Ghebache<sup>3</sup>, Moustafa M.S. Sanad<sup>4,\*</sup>, Aldjia Aitouakli<sup>5</sup>, Zineb Meguellati<sup>2</sup>

<sup>1</sup> Laboratory of Applied Chemistry and Materials (LabCAM), University of M'hamed Bougara of Boumerdes, Avenue de l'Indépendance, Boumerdes, 35000, Algeria

<sup>2</sup> Fibrous Polymer Processing and Shaping Laboratory, M'Hamed Bougara University of Boumerdes, Avenue de l'Indépendance, Boumerdes, 35000, Algeria

<sup>3</sup> Macromolecular Synthesis and Thio-Organic Macromolecular Synthesis Laboratory, USTHB, Algeria

<sup>4</sup> Central Metallurgical Research & Development Institute, P.O. Box: 87 Helwan, 11421, Cairo, Egypt

<sup>5</sup> IAP / Algerian Petroleum Institute, Avenue du 1er Novembre 1954, Boumerdes, Algeria.

\*Corresponding author: Email: [mustafa\\_sanad2002@yahoo.com](mailto:mustafa_sanad2002@yahoo.com), (Moustafa M.S. Sanad)

Received.....28 April 2025

Accepted.....17 June 2025

Published.....30 June 2025

## Abstract

The increasing demand for sustainable energy is one of the major challenges facing the industrial sector in recent times, which results in a constant need to search for new, simple, low-cost, and effective materials. In this prospective, homogeneous and stable electrode materials based on PPy/TiO<sub>2</sub> films on ITO glass substrate were electrochemically synthesized from aqueous medium. The electrodeposited films are structurally characterized and morphologically scanned using different spectroscopic and micro-spectroscopic techniques including X-ray diffraction (XRD), Fourier Transform Infra-Red (FTIR), and Field Emission Scanning Electron Microscope (FESEM), respectively. The light absorbance and photocurrent-potential measurements confirmed the synergistic effect of the oxide@conductive-polymer combination. The electronic conduction properties of TiO<sub>2</sub>/PPy deposited films were also studied; the best specific capacitance values of PPy films were achieved after 50 cycles of voltammetric deposition at 50 mV.s<sup>-1</sup> with an oxidation current response of 4.75 mA and specific capacitance ~ 180 F.g<sup>-1</sup>. A remarkable increase in specific capacity was obtained as a result of the incorporation of 10% anatase nanoparticles into the PPy matrix up to 250 F.g<sup>-1</sup>. Faster charge-discharge rates lead to the reduction of adsorbed ions on the electrode surface, causing lower specific capacitance. Asymmetric supercapacitive cells of PPy@ITO and TiO<sub>2</sub>/PPy@ITO demonstrated excellent stability and capacity retention, reaching up to 85% and 97.1%, respectively, after 1000 multiple cycles. The impedance measurements performed in the domain of 10 kHz to 10 mHz indicated that TiO<sub>2</sub>/PPy@ITO composite (~ ratio 0.1) has the lowest values of electrochemical resistance parameters in terms of the electrolyte, charge transfer, and ions diffusion from the electrolyte into the electrode surface.

**Keywords:** Electropolymerization; Galvanostatic Cycling; Polypyrrole/TiO<sub>2</sub>; Specific Capacitance.

## 1. Introduction

In recent years, the development of novel materials for sustainable energy has emerged as a major focus for many research groups [1-4]. Consequently, much attention has been paid to energy sources, especially electrochemical capacitors and supercapacitors, as a

potential energy storing technology due to their large power density, fast charge/discharge rates, and exceptional cycling stability [5-8]. These unique characteristics can be achieved when an electrode material with a high specific surface area is paired with

a substance capable of undergoing reversible oxidation and reduction across a broad potential range [9]. Therefore, the quality of a supercapacitor can be established if the electrode material is (i) voltammetrically stable at a broad range of sweep rates; (ii) capable of producing high power densities and (iii) has the lowest equivalent series resistance (ESR) [10, 11]. Carbon-based materials were among the first to be employed in industrial supercapacitors because of their excellent cycle stability, their large specific surface area, and their high adsorptive capacity in the concentration of charges at the interface between the electrode and the electrolyte [12]. However, these materials display several drawbacks, such as high internal resistance due to the contact between the carbon particles, high micro-porosity, and that their surface area is inaccessible for large-sized electrolytic ions, which reduces their electrochemical performance [13]. Previous studies have focused on the polypyrrole (PPy) as a robust foundation for supercapacitive electrodes owing to its good redox activity and excellent electrical conductivity [14, 15]. However, the lifespan of PPy as a conductive polymer is still limited due to the volumetric changes in the structure (swelling) during redox reactions, which lead to evolution or even degradation of these active materials [16]. Accordingly, the combination of conducting polymers and metal oxides has garnered significant attention for its synergistic effects, causing a significant enhancement in the overall electrochemical performance [17]. In particular, the polypyrrole/metal oxide hybrid system represents a compelling class of materials in the realm of supercapacitor technology [18, 19]. Clearly, the incorporation of ZnO, RuO<sub>2</sub> and MnO<sub>2</sub> nanomaterials with large faradic pseudocapacity into polypyrrole exhibited a unique set of electrochemical properties that exceeded those of individual components [20, 21]. They also contributed to improved charge storage capacity, electrical conductivity, and structural stability [22, 23].

In particular, the incorporation of TiO<sub>2</sub> in the conducting polymer composite is more favorable for many reasons, including the non-toxicity, cost-effectiveness, high mechanical stability, improved light absorptivity, high efficiency of e/h separation and suitable channels for hybrid electrochemical storage mechanisms [24-27]. However, there are many methods that have been used to manufacture these types of materials, among which the electrochemical process was chosen for this study because it has many advantages including ease of synthesis, adhesion strength, decoration, long-term conductive stability and low cost. [28-31].

Based on the above, the aim of this study is to improve the performance of electrochemically synthesized TiO<sub>2</sub>/polypyrrole films on glass plates containing a thin layer of indium tin oxide (ITO) sheets. The polymerization of pyrrole was electrochemically performed by cyclic voltammetry (CV) at different number of cycles and scanning speeds. The changes in the structure and morphology of different TiO<sub>2</sub>/PPy composites with addition of different loads of TiO<sub>2</sub> particles were inspected by X-ray diffraction (XRD), Fourier transmission infra red (FTIR) and scanning electron microscopy (SEM).

The electronic/photoconduction and electrochemical properties of these hybrid systems were evaluated using several techniques of UV-Visible spectroscopy, CV, galvanostatic/constant-current charge-discharge testing (GCD) and electrochemical impedance analysis (EIS).

## 2. Experimental part

### 2.1. Materials and characterization

The pure chemicals of anatase type (TiO<sub>2</sub>, 99%), Pyrrole (99%), anhydrous ferric chloride (FeCl<sub>3</sub>, 99%) and sulphuric acid (H<sub>2</sub>SO<sub>4</sub>, 98%) were purchased from Sigma Aldrich. A high laboratory grade of deionized water was employed through the whole experiments. X-ray diffraction (XRD) measurements were performed using a PANalytical X'Pert Pro diffractometer equipped with a Cu K $\alpha$  radiation source. FTIR spectrometer type 8400 SHIMADZU was utilized for studying the functional characteristics of raw materials and electrodeposited films. The electrochemical deposition and measurements were performed using an Autolab device PGSTAT302N MBA integrated with NOVA 1.7 software. A Field Emission Scanning Electron Microscope (FESEM, Phillips XL 30 model) was employed to examine the microstructure of both pure PPy and TiO<sub>2</sub>/PPy composite films. The UV-Visible absorption spectra for pure PPy and TiO<sub>2</sub>/PPy films of different ratios (0.05-0.15) were recorded from SHIMADZU 1601 UV-Visible Spectrophotometer.

### 2.2. Electrodeposition and capacitive measurements

All electrochemical measurements were performed using an Autolab PGSTAT302N MBA instrument integrated with NOVA 1.7 software. The three-electrode setup cell consists of ITO-glass as working electrode, platinum wire as counter electrode and reference calomel electrode Hg/Hg<sub>2</sub>Cl<sub>2</sub> immersed in saturated KCl (SCE). The electrochemical synthesis was conducted in an aqueous solution containing 0.1M H<sub>2</sub>SO<sub>4</sub> (9.81 g/L) and 0.01M Pyrrole (0.67 g/L), while the capacitance measurements were carried out in a solution of 0.1M H<sub>2</sub>SO<sub>4</sub> (9.81 g/L) [32]. The

electrodeposition experiment consists of two steps: first, polymerization of polypyrrole only, and then formation of the conductive TiO<sub>2</sub>/PPy composite polymer films on the surface of the ITO-glass. The employed plates of ITO-glass were cleaned in an ultrasonic bath of acetone for 15 min, then dried out at 60°C for 1 h. The active surface area was adjusted to 1 cm<sup>2</sup> using Teflon tape of the conductive side. The ITO-glass plates were weighed before and after each electrochemical polymerization. The polymerization of pyrrole was electrochemically performed by repetitive cyclic voltammetry (CV) at different scanning speeds. The coated film for each sample was obtained after 50 cycles at scanning speeds of 50 mV.s<sup>-1</sup>. For capacitance measurements, the CVs cycles for the fabricated films were conducted in the potential window from -0.6V to 0.8V and at scanning speeds from 5 to 200 mV.s<sup>-1</sup>. A series of experiments were performed in order to determine the best mass ratio of TiO<sub>2</sub>/PPy required to obtain a better reinforcement / polymer matrix deposit with high capacitance, which will in turn be used as high introductions in supercapacitors.

The specific capacitance was determined using the following relation:

$$\text{Specific capacitance (Cs)} = \frac{1}{S_r(V_c - V_a) \cdot S} \int_{V_a}^{V_c} I(V) dV \quad \text{..... (Eq. 1) [17]}$$

where  $S_r$  denotes to the scan rate (mV. S<sup>-1</sup>);  $V_c - V_a$  (potential range);  $I (V)$  the current density response (A.cm<sup>-2</sup>), and  $S$  to the area of the ITO plate.

After the optimization of the synthesis conditions of the polypyrrole deposition, a second optimization was performed for the synthesis of the conductive polymer composite films based on TiO<sub>2</sub>/PPy. For this purpose, various experiments were conducted in order to determine the best mass ratio of TiO<sub>2</sub>/PPy required to obtain a better reinforcement / polymer matrix deposit with high capacitance, which will in turn be used as high introductions in supercapacitors.

### 3. Results and discussions

#### 3.1. Electrochemical manufacturing of films

CV is an effective method for rational engineering of PPy and TiO<sub>2</sub>/PPy conductive coatings on ITO substrate through electrochemical polymerization process. Fig. 1a and b display the effect of repetitive CVs for ITO electrodes in the existence of pyrrole and (b) TiO<sub>2</sub>/ pyrrole in 0.1 M H<sub>2</sub>SO<sub>4</sub> at 50 mV.s<sup>-1</sup>, respectively. The CVs curves of these systems show the appearance of anodic/cathode electron transfer only in the first cycles. As the number of sweeps increases, these peaks are fully vanished. This trend is interpreted

as the first step of oxidation of the pyrrole monomer was slow, hence the formation of a cation radical followed by the formation of a dimer as a result of the addition reaction which can be observed as anodic/cathode peaks [33]. After the formation of the dimers, and as the CVs continue, the anode/cathode peaks completely disappear. This is due to the fact that the oxidation potentials of the dimers are lower than that of the monomers, resulting in faster polymer growth. It is worth noting that no significant changes were detected when anatase was added to the system, which may be due to the dominance of the electro-polymerization process over the co-deposition reaction.

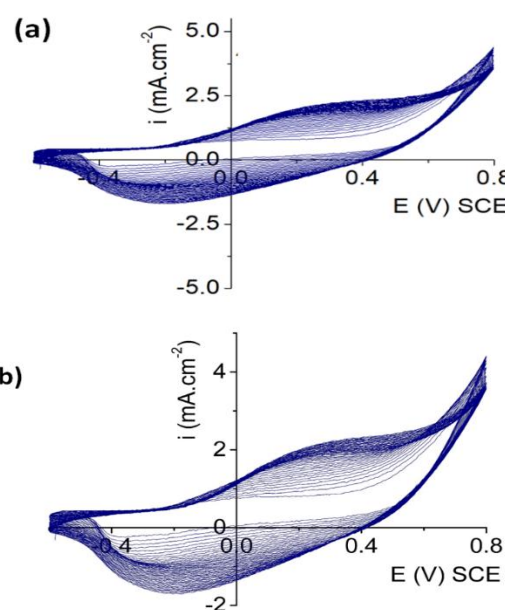


**Fig. 1** Cyclic voltammograms (CVs) of ITO electrodes in the presence of (a) PPy, and (b) TiO<sub>2</sub>/PPy in 0.1 M H<sub>2</sub>SO<sub>4</sub> for 50 cycles at 50 mV.s<sup>-1</sup>.

#### 3.2. Structural characterization

To investigate the crystallinity and structure of the electropolymerized films, the XRD patterns of pure PPy/ITO and co-deposited TiO<sub>2</sub>-PPy/ITO samples were compared with powdered TiO<sub>2</sub>, as shown in Fig. 2a. The XRD data profile of bulk TiO<sub>2</sub> exhibits five sharp peaks at 2 $\theta$  angles around 25.25 °; 37.95 °; 48.11 °; 53.88 ° and 55.10 ° which correspond to (101), (004), (200), (105) and (211) diffraction planes of the anatase phase. The diffraction curve of PPy indicates a broad peak in the 20-30° range because the formed PPy deposit is amorphous [34]. In addition, the XRD profile of TiO<sub>2</sub>/PPy composite film demonstrates overlapping between the main peaks of anatase and the broad diffraction peak of PPy, confirming the successful deposition of TiO<sub>2</sub>/PPy film on the surface of ITO substrate [35]. In order to ensure the smooth running of

the polymerization process, we characterized the electro-synthesized polymer by FTIR spectroscopy. The characteristic transmission bands of the polypyrrole structure are shown in Fig. 2b. The broad band that appeared at  $1700\text{ cm}^{-1}$  is attributed to the adsorbed water [36]. The absence of bands around  $1550$  and  $1467\text{ cm}^{-1}$  is evidence for the non-vibration of bond. The band at  $1287\text{ cm}^{-1}$  indicates the vibration in the bonding plane of CH bond. The band appearing at  $1191\text{ cm}^{-1}$  is related to the vibration of the NC bonds. The vibrational mode at  $1106\text{ cm}^{-1}$  is attributed to  $\text{HSO}_2^-$  or the anion  $\text{SO}_2^{2-}$  linked to the doped state of PPy. The deformation vibration in the plane of the NH bonds appeared at  $1044\text{ cm}^{-1}$ . The weak absorption peaks of polypyrrole that appeared at  $962$ ,  $912$  and  $786\text{ cm}^{-1}$  are related to the deformation vibrations of C = C, C-H and N-H bonds in the pyrrole ring outside the plane [36, 37]. The infrared spectra of pure anatase sample show a wide and strong absorption band between  $1200\text{ cm}^{-1}$  and  $500\text{ cm}^{-1}$  which are attributed the vibration of Ti-O and Ti-O-Ti bonds [38]. The peak at  $1622\text{ cm}^{-1}$  is attributed to the bending of the OH groups of adsorbed  $\text{H}_2\text{O}$  molecules on the surface of  $\text{TiO}_2$  [39]. The middle FTIR spectra shows the weakness of  $\text{TiO}_2$  bands which confirms the success of the electrochemical polymerization reaction of pyrrole molecules and the formation of PPy around the  $\text{TiO}_2$  particles.

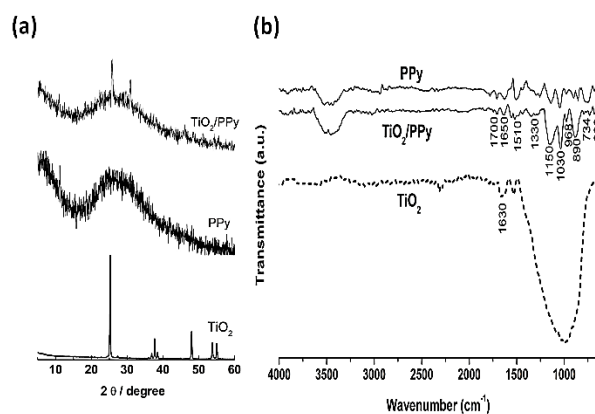


**Fig. 2** XRD patterns (a) and FTIR spectra (b) of bulk  $\text{TiO}_2$  and the fabricated PPy/ITO and  $\text{TiO}_2$ /PPy/ITO films (0.1 molar ratio).

Figures 3 a and b indicate the SEM images of the electrodeposited PPy film, showing the homogeneous bended sheets of the polymer at different magnifications. Meanwhile, Fig. 3c and d shows the homogenous distribution of  $\text{TiO}_2$  particles in the PPy matrix. Figure 4a displays the UV-Visible spectra for the electrodeposited films with several  $\text{TiO}_2$ /PPy mass ratios, namely 0.05 - 0.08 - 0.1 and 0.15 prepared after 50 voltammetric cycles under a scanning speed of  $50\text{ mV}\cdot\text{s}^{-1}$  in a  $0.1\text{ M H}_2\text{SO}_4$  medium.

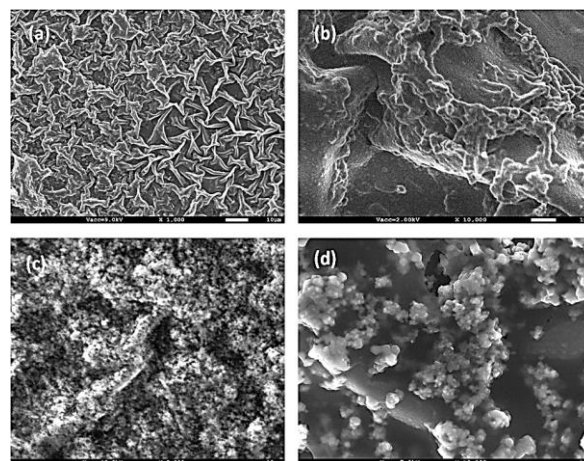


**Fig. 3** SEM micrographs of the electrochemically engineered films (a, b) PPy/ITO and (c, d) PPy/ $\text{TiO}_2$ /ITO at different magnifications

50 voltammetric cycles under a scanning speed of  $50\text{ mV}\cdot\text{s}^{-1}$  in a  $0.1\text{ M H}_2\text{SO}_4$  medium. The optical absorption of the PPy indicates the appearance of a characteristic band of PPy between  $200$  and  $300\text{ nm}$  which is due to the electron transition ( $\pi \rightarrow \pi^*$ ) from the highest occupied molecular orbital (HOMO) to the lowest unoccupied molecular orbital (LUMO) in the case of short conjugated PPy [40]. Another absorption band was observed between  $300$  and  $500\text{ nm}$ , which was attributed to the polaron, which is confined to a specific number of rings [34]. The optical absorbance spectra of  $\text{TiO}_2$ /PPy with mass ratio  $\sim 0.05$  and  $0.08$ , show better absorption than ITO but are still lower than pure PPy. However, with increasing  $\text{TiO}_2$  content up to the mass ratio of  $\text{TiO}_2$ /PPy  $\sim 0.1$ , the absorptivity reaches the equilibrium state with pure PPy. The photocurrent response under visible light and darkness for these various deposited films is also studied as shown in Fig. 4b. It is obvious that a clear improvement in the faradic current value of the  $\text{TiO}_2$ /PPy-based deposited films under the visible light irradiation reaching to  $3.52\text{ }\mu\text{A}\cdot\text{cm}^2$  compared to its individual components of PPy ( $3.3\text{ }\mu\text{A}\cdot\text{cm}^2$ ) and  $\text{TiO}_2$  ( $2.98\text{ }\mu\text{A}\cdot\text{cm}^2$ ). Similar results are also observed in the dark conditions. Fig. 4b shows Photocurrent-potential responses of PPy/ $\text{TiO}_2$ @ITO electrodes under visible light and dark conditions.

The results demonstrate that a peak appears when there is irradiation of visible light, and disappears when the irradiation is removed, which is due to the photoelectric properties of the materials. The current densities of  $\text{TiO}_2$ /PPy@ITO,  $\text{TiO}_2$ @ITO and PPy@ITO electrodes are  $1.4$ ,  $0.2$  and  $0.4\text{ }\mu\text{A}\cdot\text{cm}^{-2}$ , respectively. It is noticeable that the current value of  $\text{TiO}_2$ /PPy@ITO electrode is the highest, indicating that this electrode is the best in terms of the generation, separation, and transfer efficiency of electron-hole

pairs. These results can also indicate the synergistic effect of the oxide and the semiconductor for the enhancement of TiO<sub>2</sub> photoelectrochemical properties.

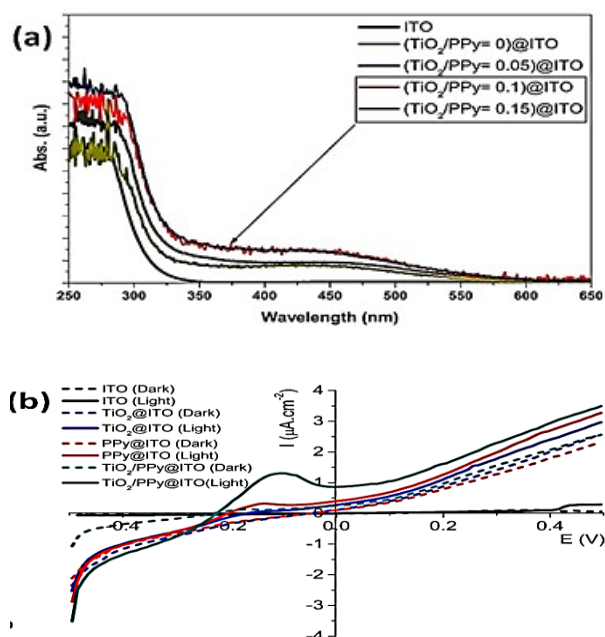


**Fig. 4** (a) UV-Vis absorption spectra of PPy/TiO<sub>2</sub>/ITO deposited films with different weight ratio 0-0.15, and (b) Photocurrent-potential responses of PPy/TiO<sub>2</sub>@ITO electrode and its individual components under visible light and dark conditions.

### 3.3. Capacitive measurements

Figure 5a depicts the CVs of the deposited polypyrrole films after 50 polarization cycles at various scan speeds (5-200 mV.s<sup>-1</sup>) in an aqueous electrolyte based on 0.1 M H<sub>2</sub>SO<sub>4</sub> versus SCE and Pt wire as reference and auxiliary electrodes, respectively. It can be seen that the PPy films exhibit non-rectangular CV curves a distinct pair of redox peaks around 0.3/0.4 V, which are typical of the oxidation and reduction of PPy. The best electrochemical response is obtained with a scan speed of 5 mV.s<sup>-1</sup> with an oxidation current response of 4.75 mA and specific capacitance ~ 180 F.g<sup>-1</sup> (30 mF.cm<sup>-2</sup>). Fig. 5b shows the relationship between the calculated specific capacitance and scan rates. The specific capacitance linearly decreases with increasing scan rate due to the reduction of adsorbed ions on the electrode surface.

Meanwhile, the corresponding CVs of the deposited TiO<sub>2</sub>/PPy (mole ratio ~ 0.1) at various scan speed ranges (5-200 mV.s<sup>-1</sup>) are illustrated in Fig. 6a. It can be noted that the oxidation peaks have weak offsets before the introduction of TiO<sub>2</sub> nanoparticulate fillers. This higher polarization can be observed than in the films made of PPy alone because the formation of thick

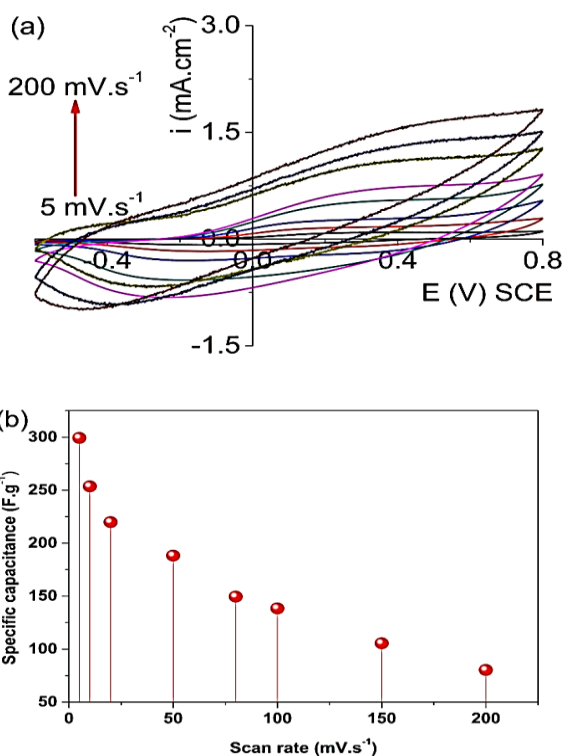


**Fig. 5** (a) CVs of asymmetric supercapacitor of the electrochemically fabricated PPy@ITO films, and the corresponding (b) Specific capacitance at different scanning rates from 5 to 200 mV.s<sup>-1</sup>

C-C layer which reduce the specific capacitance values, suggesting that the prepared composite films could be more suitable for the application in supercapacitors [41]. Fig. 6b illustrates the impact of faster charge-discharge rates on the supercapacitive performance of TiO<sub>2</sub>/PPy composite films with different mole ratios (0.0, 0.05, 0.1, and 0.15).

The largest specific capacitance of about 250 F.g<sup>-1</sup> (43 mF.cm<sup>-2</sup>) is achieved with the mole ratio 0.1 of TiO<sub>2</sub>/PPy composite, which means that the divalent SO<sub>4</sub><sup>2-</sup> and monovalent HSO<sub>4</sub><sup>-1</sup> ions are highly adsorbed on the microporous surface of this composite ratio. However, the observed reduction in the specific capacitance by increasing the TiO<sub>2</sub> up to 0.15 mole ratio could be ascribed to the increase in the electrode resistance, which causes a limitation to the ionic transport kinetics between the electrolytes and the electrode surface. In other words, the diffusion of sulphate ions through the TiO<sub>2</sub>/PPy composite is more favored than the case of PPy itself. The reason for this behavior is the polymer nanocomposite films' conductivity and rapid charge transfer between the hydrogen atoms of PPy and the oxygen atoms of TiO<sub>2</sub> nanoparticles via weak hydrogen bonds [42].

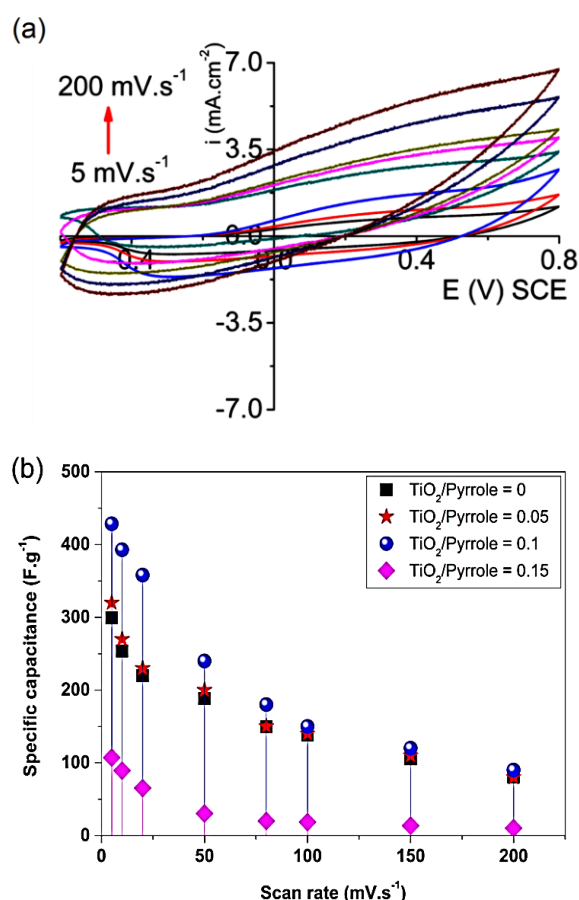


Fig. 6: (a) CVs of asymmetric supercapacitor of the electrochemically designed TiO<sub>2</sub>/PPy@ITO with ratio 0.1, and (b) Comparison for the corresponding specific capacitance of TiO<sub>2</sub>/PPy@ITO electrodes with different ratio 0-0.15 at different scanning rates from 5 to 200 mV.s<sup>-1</sup>

Figure 7 displays the successive CVs for the electrodeposition of TiO<sub>2</sub>/PPy in 0.1 M H<sub>2</sub>SO<sub>4</sub> at 50 mV.s<sup>-1</sup> and the correspond CVs of asymmetric supercapacitor of the electrochemically designed TiO<sub>2</sub>/PPy@ITO at different scanning rates from 5 to 200 mV.s<sup>-1</sup> with TiO<sub>2</sub>/PPy mole ratio (a) 0.05 and (b) 0.15, respectively. Results confirms that the sample with mole ratio 0.05 gives slightly higher capacitance than pure PPy film, while the sample 0.15 mole ratio has lower specific capacitance as previously depicted in Fig. 6.

Figure 8 compares the cyclability study of the prepared PPy@ITO and TiO<sub>2</sub>/PPy@ITO (mass ratio 0.1) films prepared through multiple voltammetric deposition at 50 mV.s<sup>-1</sup>. Obviously, the cell of TiO<sub>2</sub>/PPy@ITO shows better capacitance retention, keeping 97% of its initial capacitance after 1000 oxidation reduction cycles with 100 mV.s<sup>-1</sup>. On the other hand, the cell of prepared PPy@ITO preserves about 72% of its initial capacitance after 1000 cycles.

This could be explained by the enhanced mechanical stability and good electronic conductivity of composite compared to the PPy alone. The obtained results show good agreement with physicochemical characterization findings.

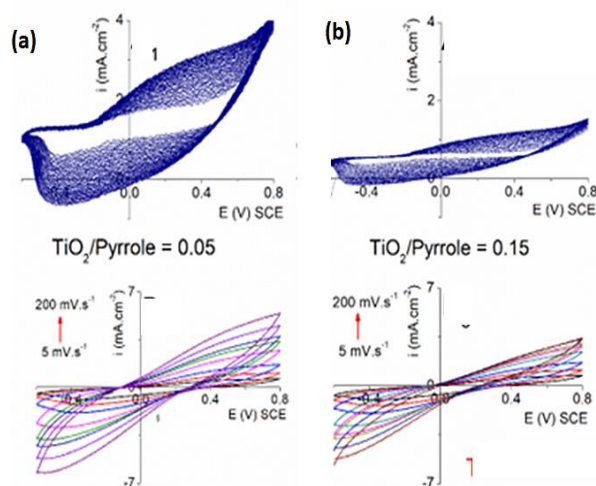


Fig. 7 Multiple CVs for the electrodeposition of TiO<sub>2</sub>/PPy in 0.1 M H<sub>2</sub>SO<sub>4</sub> at 50 mV.s<sup>-1</sup> and the corresponding CVs of asymmetric supercapacitor of the electrochemically designed TiO<sub>2</sub>/PPy@ITO at different scanning rates from 5 to 200 mV.s<sup>-1</sup> with TiO<sub>2</sub>/PPy mole ratio (a) 0.05 and (b) 0.15, respectively

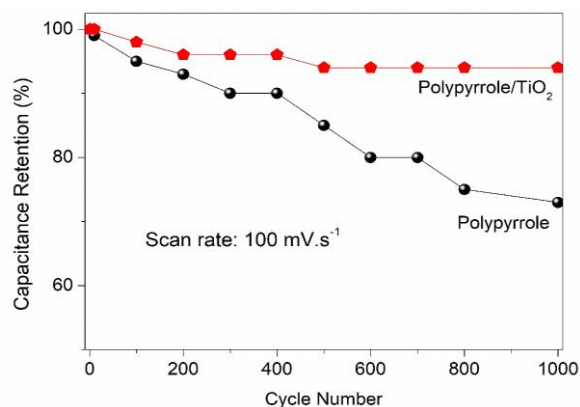
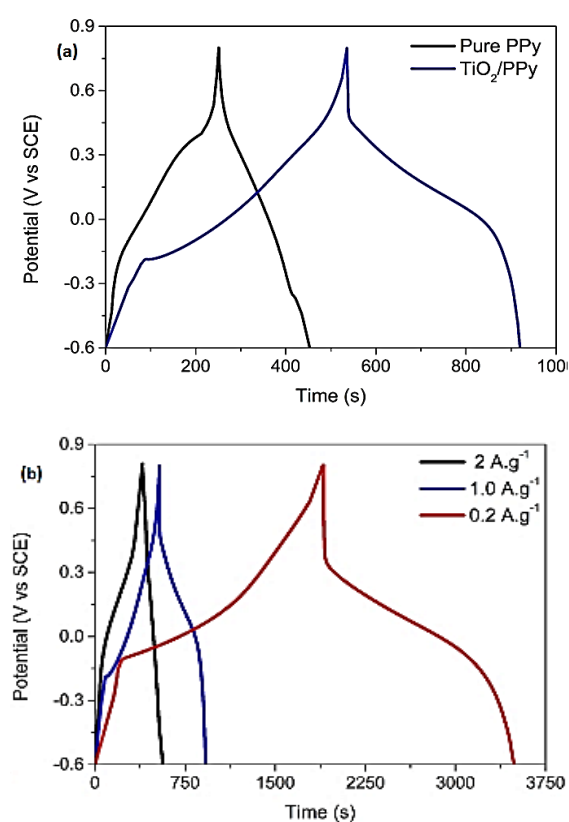


Fig. 8 Cyclability of PPy@ITO and TiO<sub>2</sub>/PPy@ITO (mass ratio 0.1) at 100 mV.s<sup>-1</sup> scan rate.

Figure 9a depicts the GCD profiles of PPy@ITO and TiO<sub>2</sub>/PPy@ITO (mass ratio 0.1) at 1 mA. The calculated values of specific capacitance for PPy@ITO and TiO<sub>2</sub>/PPy@ITO are equal to 120 and 160 F.g<sup>-1</sup>, respectively. The noticeable improvement in the capacitance of TiO<sub>2</sub>/PPy@ITO shows a good agreement with the capacitance results obtained by cyclic voltammetry graphs. It is also noticed that the TiO<sub>2</sub>/PPy@ITO has the longest voltage plateaus as

revealed in charge/discharge processes, which confirms the electrochemical activity of the composite electrode compared to the pure PPy electrode. Besides, the equal length of both oxidation and reduction curves in the composite indicate the stability and good adherence of ions compared to the adsorbed ions over PPy surface which oxidized faster than reduction, suggesting bad reversibility. Fig. 9b shows the GCD profiles of TiO<sub>2</sub>/PPy@ITO (mass ratio 0.1) at different current densities (0.2, 1.0, and 2 A.g<sup>-1</sup>). It is found that specific capacitance noticeably improved by decreasing the current density to reach about 350 F.g<sup>-1</sup> at 0.2 mA.



**Fig. 9** (a) Galvanostatic charge-discharge (GCD) profiles of PPy@ITO and TiO<sub>2</sub>/PPy@ITO (mass ratio 0.1) at a current density of 1 A.g<sup>-1</sup>, and (b) GCD profiles of TiO<sub>2</sub>/PPy@ITO (mass ratio 0.1) at different current densities (0.2, 1.0, and 2 A.g<sup>-1</sup>).

Moreover, the galvanostatic cyclic performance of both electrodes up to 1000 successive cycles at 0.2 mA is represented in Fig. 10. Both PPy@ITO and TiO<sub>2</sub>/PPy@ITO cells demonstrates excellent stability and capacity retention reaching up to 85% and 97.1%, respectively after 1000 multiple cycles.

The reason for such improvement can be clearly justified by studying the values of EIS in the frequency range from 10 kHz to 10 mHz. It is worth to note that

the prepared TiO<sub>2</sub>/PPy film achieved higher specific capacitance (350 F.g<sup>-1</sup>) than previously prepared TiO<sub>2</sub>/PPy (~ 150 F.g<sup>-1</sup>) by S. Ha et al [43]. Meanwhile, succeeded in preparing Moiré-like TiO<sub>2</sub>/PPy electrodes with very close electrocapacitive performance (~ 355 F.g<sup>-1</sup>) [44].

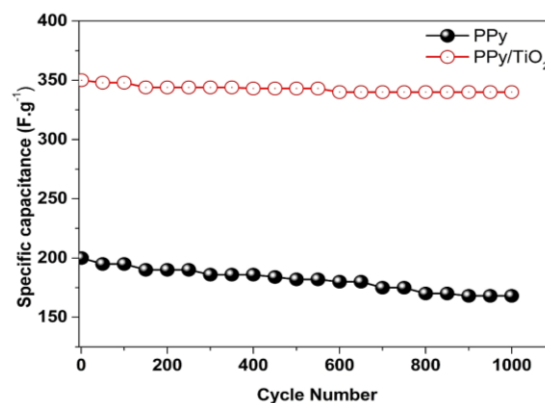


**Fig. 10** Cycle life performance of PPy@ITO and TiO<sub>2</sub>/PPy@ITO (mass ratio 0.1) at 0.2 A.g<sup>-1</sup>.

The impedance measurements are presented by the Nyquist plots in Fig. 11, and the fitted data used the inserted equivalent circuit. As depicted in Fig. 11, the cell of TiO<sub>2</sub>/PPy@ITO composite electrode has the lowest electrochemical resistance values for the electrolyte (R1), charge transfer (R2) and ionic diffusion from the electrolyte into the electrode surface (W2). Accordingly, the improved values of EIS parameters suggest the enhancement in the cyclic stability and charge carriers' mobility by the inclusion of TiO<sub>2</sub> particles.

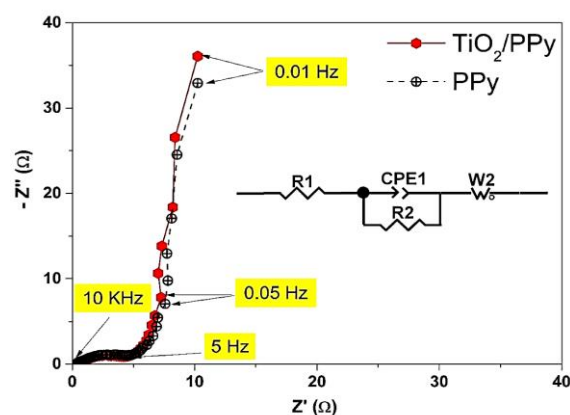


**Fig. 11** EIS spectra of PPy@ITO and TiO<sub>2</sub>/PPy@ITO (mass ratio 0.1).

## Conclusions

This work focuses on the electrochemical synthesis and characterization of conductive composite films on ITO sheets through encryption of anatase nanoparticles into PPy matrix to improve its capacitive performance in supercapacitors. XRD and FTIR results confirmed the successful deposition of TiO<sub>2</sub>/PPy film with different molar ratios on the surface of ITO substrate. SEM observation of the electrochemically synthesized TiO<sub>2</sub>/PPy composite revealed the encapsulation of TiO<sub>2</sub> spherical particles with PPy sheets forming a mesoporous and homogenous layer on ITO. The prepared TiO<sub>2</sub>/PPy films showed higher values of the photo-current response compared to their individual components under visible light irradiation. The film composite of TiO<sub>2</sub>/PPy with ratio ~ 0.1 indicated the best capacitive performance among all composite ratios due to the enhanced diffusion of electrolyte ions on the surface of the electrode material and the retardation of bulging phenomenon in PPy. The successive galvanostatic cycling tests for 1000 cycles tests indicated the excellent stability of the composite film in comparison to pure PPy. The lowest electrochemical resistance values for the electrolyte (R1), charge transfer (R2), and ion diffusion from the electrolyte into the electrode surface (W2) are found in the cell of the TiO<sub>2</sub>/PPy@ITO composite electrode.

## References

- [1] F. Hamidouche, Z. Ghebache, J. Lepretre and N. Djelali, Montmorillonite/Poly(Pyrrole) for Low-Cost Supercapacitor Electrode Hybrid Materials, *Polymers*, 16: 919 (2024)
- [2] A. S. Ghanem, F. Liang, M. Liu, H. Jiang, A. Toghan, Hydrogen production by water splitting coupled with the oxidation of coke oven gas in a catalytic oxygen transport membrane reactor, *Chemical Engineering Journal*, 474: 145263 (2023).
- [3] M. M. S. Sanad, N. K. Meselhy, M. S. Eraky, A. Toghan, One-pot synthesis of TiO<sub>2</sub>-decorated SnSe/ZnS as a novel anode material with promoted storage capacity and cyclability in lithium-ion batteries, *J. Mater. Sci.: Mater. Electron.* 35: 850 (2024).
- [4] M. Sanad, A. Toghan, Chemical activation of nanocrystalline LiNbO<sub>3</sub> anode for improved storage capacity in lithium-ion batteries, *Surfaces and Interfaces*, 27: 101550 (2021).
- [5] N. A. Elessawy, S. A. Al-Hussain, A. Toghan, Engineering of Pt@Ni,N-doped graphene electrocatalyst based on recycled water bottles waste as an efficient cathode material for PEM fuel cells, *Diam. Relat. Mater.* 146: 111204 (2024).
- [6] M M S Sanad, S W Arafat, Z K Heiba, A Toghan, and A I Alakhras, Fabrication of Ni<sub>3</sub>S<sub>2</sub>-functionalized V<sub>2</sub>O<sub>3</sub> nanospheres as promising anode materials for rechargeable batteries and supercapacitors, *Appl. Phys. A* 129: 516 (2023).
- [7] M. M. S. Sanad, N. K. Meselhy, H. A. El-Boraey, A. Toghan, Controllable engineering of new ZnAl<sub>2</sub>O<sub>4</sub>-decorated LiNi<sub>0.8</sub>Mn<sub>0.1</sub>Co<sub>0.1</sub>O<sub>2</sub> cathode materials for high performance lithium-ion batteries, *Journal of Materials Research and Technology* 23: 1528-1542 (2023).
- [8] V. Molahalli, V. S. Bhat, A. Shetty, D. Hundekal, A. Toghan, G. Hegde, ZnO doped SnO<sub>2</sub> nano flower decorated on graphene oxide/polypyrrole nanotubes for symmetric supercapacitor applications, *J. Energy Storage* 69: 107953 (2023).
- [9] C Zhan, X Zeng, X Ren, Y Shen, R Lv, F Kang et al Dual-ion hybrid supercapacitor: Integration of Li-ion hybrid supercapacitor and dual-ion battery realized by porous graphitic carbon, *J. Energy Chem.* 42: 180–184 (2020).
- [10] X. Zhao, B. M. Sánchez, P. J. Dobson, and P. S. Grant, “The role of nanomaterials in redox-based supercapacitors for next generation energy storage devices, *Nanoscale.* 3: 839–855 (2011).
- [11] R. Ramya, R. Sivasubramanian, and M. V. Sangaranarayanan, “Conducting polymers-based electrochemical supercapacitors - Progress and prospects, *Electrochim. Acta* 101: 109–129 (2013).
- [12] Z. Zhai, L. Zhang, T. Du, B. Ren, Y. Xu, S. Wang, J. Miao, Z. Liu, A review of carbon materials for supercapacitors, *Mater. Des.* 221: 111017 (2022).
- [13] Kumar R, Joanni E, Sahoo S, Shim J, Tan W K, Matsuda A et al, An overview of recent progress in nanostructured carbon-based supercapacitor electrodes: From zero to bi-dimensional materials, *Carbon.* 193: 298-338 (2022).
- [14] H Y Kalyon, M Gencten, S Gorduk, Y Sahin, Novel composite materials consisting of polypyrrole and metal organic frameworks for supercapacitor applications, *J. Energy Storage.* 48: 103699 (2022).
- [15] J. Liu, Y. Liu, T. Li, L. Liang, S. Wen, Y. Zhang, G. Liu, F. Ren, G. Wang, Efficient Regulation of Polysulfides by Anatase/Bronze TiO<sub>2</sub> Heterostructure/Polypyrrole Composites for High-Performance Lithium-Sulfur Batteries. *Molecules*, 28: 4286 (2023).

- [16] Y Tian, C Yang, X Song, J Liu, L Zhao, P Zhang et al, Engineering the volumetric effect of Polypyrrole for auto-deformable supercapacitor, *Chem. Eng. J.* **374**: 59-67 (2019).
- [17] Z Ghebache, F Hamidouche, Z Safidine, M Trari, and B Bellal, *J. Inorg. Organomet. Polym. Mater.* **29** 1548–1558 (2019).
- [18] F Hamidouche, M M S Sanad, Z Ghebache, and N Boudieb, Synthesis and Electrical Conducting Properties of Poly(aniline) Doped With Zeolite HY Nanocomposites Containing SnO<sub>2</sub> for High-Performance Supercapacitor Electrode, *J. Mol. Struct.* **1251**: 131964 (2022).
- [19] N. Boutaleb, G. M. Al-Senani, S. D. Al-Qahtani, A. Benyoucef, B. D. Alkoudsi, Investigation and properties of PANi-coated CuO–ZnO–MnO quaternary hybrid as electrode material for supercapacitor application, *Colloids and Surfaces A: Physicochemical and Engineering Aspects*, 718: 136867 (2025).
- [20] L M Huang, H Z Lin, T C Wen, and A Gopalan, Highly dispersed hydrous ruthenium oxide in poly(3,4-ethylenedioxythiophene)-poly(styrene sulfonic acid) for supercapacitor electrode, *Electrochim. Acta.* **52**:1058 – 1063 (2006).
- [21] R K Sharma, A C Rastogi, and S B Desu, Manganese oxide embedded polypyrrole nanocomposites for electrochemical supercapacitor, *Electrochim. Acta.* **53**: 7690–7695 (2008).
- [22] C Wang, Z Liu, Q Wang, J Guo, Q Zhao, and Y Lu, MnO<sub>2</sub>@polypyrrole composite with hollow microsphere structure for electrode material of supercapacitors, *J. Electroanal. Chem.* **901**: 115780 (2021).
- [23] M M Moharam, M M S Sanad, E M El-Sayed, and M E Ibrahim, Power Saving Electrochemical Processing of Low Cost MnO<sub>2</sub>@Porous Al Electrode for High Performance Supercapacitors Applications, *IOP CONF. SER. MATER. SCI. ENG.* **762**: 012002 (2020).
- [24] J. Liu, Y. Liu, T. Li, L. Liang, S. Wen, Y. Zhang, G. Liu, F. Ren, G. Wang, Efficient Regulation of Polysulfides by Anatase/Bronze TiO<sub>2</sub> Heterostructure/Polypyrrole Composites for High-Performance Lithium-Sulfur Batteries. *Molecules*, 28: 4286 (2023).
- [25] H. Zabihi-Mobarakeh, A. Nezamzadeh-Ejehieh, Application of supported TiO<sub>2</sub> onto Iranian clinoptilolite nanoparticles in the photodegradation of mixture of aniline and 2, 4-dinitroaniline aqueous solution, *Journal of Industrial and Engineering Chemistry*, 26: 315-321 (2015).
- [26] A. Nezamzadeh-Ejehieh, M. Bahrami, Investigation of the photocatalytic activity of supported ZnO–TiO<sub>2</sub> on clinoptilolite nano-particles towards photodegradation of wastewater-contained phenol, *Desalination and Water Treatment*, 55: 1096-1104 (2015).
- [27] R. Fazaeli, H. Aliyan, A. Nezamzadeh-Ejehieh, D. Richeson, Investigation of the synergistic photocatalytic activity of a ternary ZrTiO<sub>4</sub>/TiO<sub>2</sub>/Mn<sub>3</sub>O<sub>4</sub> (ZTM) nanocomposite in a typical water treatment process, *Surfaces and Interfaces*, 52: 104877 (2024).
- [28] M. M. S Sanad, A. Toghan, Industrial perspectives for electrochemical extraction of metals from primary and secondary resources, *Inorganic Chemistry Communications* 167: 112710 (2024).
- [29] M.C. Makhloufi, L. Benhaddad, N.E. Djelali, et al. Nanofibrous PANI/TiO<sub>2</sub> Composite Synthesized with Sea Urchin-Shaped MnO<sub>2</sub> Nanostructure for High-Performance Pseudocapacitors. *Russ J Gen Chem* 93: 2360–2370 (2023).
- [30] M.S. Eraky, M.M.S. Sanad, E.M. El-Sayed, et al. Influence of the electrochemical processing parameters on the photocurrent–voltage conversion characteristics of copper bismuth selenide photoactive films. *Eur. Phys. J. Plus* 137: 907 (2022).
- [31] F. Assaf, M. Abou-krisa, T. A. Yousef, A. Abushoffa, F. El-Sheref, A. Toghan, Influence of Current Density on the Mechanism of Electrodeposition and Dissolution of Zn–Fe–Co Alloys, *Russian Journal of Physical Chemistry A* 94: 1708 (2020).
- [32] H Lyu, Triple layer tungsten trioxide, graphene, and polyaniline composite films for combined energy storage and electrochromic applications, *Polymers.* **12**: 49-65 (2020).
- [33] M. Gocki, A. Jakubowska-Ciszczek, P. Pruski, Comparative Analysis of a New Class of Symmetric and Asymmetric Supercapacitors Constructed on the Basis of ITO Collectors. *Energies* 2023, 16, 306. <https://doi.org/10.3390/en16010306>
- [34] M A Chougule, S G Pawar, P R Godse, R N Mulik, and S Sen, Synthesis and Characterization of Polypyrrole (PPy) Thin Films, *Soft Nanosci. Lett.* **01**: 6–10 (2011).
- [35] F. Gao, X Hou, A Wang, G Chu, W Wu, J Chen et al, Preparation of polypyrrole/TiO<sub>2</sub> nanocomposites with enhanced photocatalytic performance, *Particuology.* **26**: 73–78 (2016).
- [36] S Satpal, A Bhopale, P Deshpande, and A Athawale, Fabrication of ZnO-functionalized

polypyrrole microcomposite as a protective coating to enhance anticorrosion performance of low carbon mild steel, *J. Appl. Polym. Sci.* **137**: 1–9 (2020).

[37] Y Fu, Y S Su, and A Manthiram, Sulfur-Polypyrrole Composite Cathodes for Lithium-Sulfur Batteries, *J. Electrochem. Soc.* **159**: 1420-1424 (2012).

[38] M M S Sanad, E A Abdel-Aal, H M Osman, and A T Kandil, Photocatalytic reduction of hexavalent chromium with commercial Fe/Ti oxide catalyst under UV and visible light irradiation, *Int. J. Environ. Sci. Technol.* **15**: 2459–2472 (2018).

[39] A Beaussart, L Petrone, A M Vasilev, A J McQuillan, and D A Beattie, In situ ATR FTIR study of dextrin adsorption on anatase TiO<sub>2</sub>, *Langmuir.* **28**: 4233–4240 (2012).

[40] F Hamidouche, and N Djelali, Synthesis of Nanocomposites Based Semiconductors of PPy ( Cl )/ Zeolite HY, *Mater. Plast.* **52**: 437–441 (2015).

[41] E. Azizi, J. Arjomandi, H. Shi, M. A. Kiani, Flexible polypyrrole/TiO<sub>2</sub>/MXene nanocomposite supercapacitor: A promising energy storage device, *Journal of Energy Storage*, **75**: 109665 (2024).

[42] J. Arjomandi, J.Y. Lee, F. Ahmadi, M.H. Parvin, H. Moghanni-Bavil-Olyaei. Spectroelectrochemistry and electrosynthesis of polypyrrole supercapacitor electrodes based on gamma aluminum oxide and gamma iron (III) oxide nanocomposites *Electrochim. Acta*, **251**: 212-222 (2017).

[43] S. Ha, K.-Y. Shin, Fabrication of Ternary Titanium Dioxide/Polypyrrole/Phosphorene Nanocomposite for Supercapacitor Electrode Applications. *Molecules*, **29**: 2172 (2024).

[44] H. Cai, Y. Li, D. Liu, X. Yang, D. Zhou, E. Han, X. Li, Q. Li, Y. He, Construction of Moiré-like TiO<sub>2</sub>/polypyrrole electrodes for high performance photo-assisted supercapacitors, *Colloids and Surfaces A: Physicochemical and Engineering Aspects*, **703**: 135386 (2024).